tions is land of high elevation, such as exists in Antarctica, Greenland, and the Himalayas, where the landmass occupies the same altitude region as the channel 3 weighting function. Such variations, which can reach 10 to 20 K, are evident over Antarctica in Fig. 1. Only a few high mountainous regions cause variations greater than 2 K, and the effect either can be compensated for or can be ignored in these restricted areas. Channels 4 and 5 respond exclusively to the atmospheric temperature profile and are unaffected by clouds or the terrestrial surface.

The microwave data are compared with conventional meteorological data in Fig. 2, which presents preliminary estimates of thicknesses for three atmospheric layers for 5 March 1973. The 1000- to 500-mb layer is the layer of air ranging from a pressure of 1000 mb to a pressure of 500 mb. Its thickness is proportional to its average temperature; an increase of 1 K corresponds to an increase of ~20 m. The pressures 1000, 500, 250, and 50 mb roughly correspond to altitudes of 0, 5, 10, and 20 km, respectively. Temperature changes of 1 K correspond to layer thickness changes of ~20 and ~47 m for the 500- to 250-mb and 250- to 50-mb layers, respectively.

We estimated the layer thicknesses by computing for each layer an appropriate linear function of T_A for channels 3, 4, and 5, where the coefficients minimize the root-mean-square error expected for that season and region (*3*). For this purpose the globe was divided into three ocean and four land regions, the boundaries of which are indicated in Fig. 2 by small triangles. The small discontinuities in inferred layer thickness at these boundaries are thus artifacts. The depression of 80 m (~4 K) in the NEMS-inferred 1000- to 500-mb thickness which occurs near New Orleans results from a major storm with high dense clouds. Such variation is rare outside the ITCZ.

Also shown in Fig. 2 is the 1000- to 500-mb layer thickness derived from the National Meteorological Center (NMC) analyses. For most of the orbit the difference between the NMC and NEMS data is approximately 20 m or 1 K. This agreement between NMC and NEMS data suggests that microwave measurements could be a very useful source of meteorological data.

Inaccuracies in the layer thickness estimates above 500 mb are, at this time, caused principally by errors in instrument calibration and in the expressions for atmospheric transmission. Preliminary analysis of these errors suggests that increasing the pressure dependence of the 58.8-Ghz absorption coefficient significantly improves the layer thickness estimates.

Preliminary estimates of temperature profile accuracy have also been evaluated. Temperature profiles are estimated by computing, for each altitude of interest, an appropriate linear function of T_A for channels 3, 4, and 5, using the statistical procedure described earlier and an a priori global ensemble of atmospheres. Temperature profiles determined from the NEMS differ from those interpolated from selected regions of the NMC 0^h and 12^h Northern Hemisphere analyses by 1.5 to 4 K (root mean square) over the altitude range from 1 to 20 km. The largest discrepancies occur near the tropopause and at the surface where large temperature gradients are more common. These preliminary results appear to be consistent with the 0.8- to 3-K (root mean square) errors predicted for a noiseless radiometer and perfect NMC analyses.

The NEMS experiment has thus demonstrated the ability of microwave spectrometers to yield estimates of atmospheric temperature profiles in the presence of most cloud types and, over ocean, the abundances of atmospheric water vapor and liquid water. Additional information about ice and snow cover, soil moisture, and sea state is also contained in the data. It is expected that future microwave temperature-sounding systems with more frequency channels and spatial scanning will be capable of complete global coverage over the altitude range from 0 to 80 km.

D. H. Staelin, A. H. Barrett
J. W. Waters
Research Laboratory of Electronics, Massachusetts Institute of Technology, Cambridge 02139
F. T. Barath, E. J. Johnston
P. W. Rosenkranz
Jet Propulsion Laboratory, California Institute of Technology, Pasadena
N. E. Gaut
Environmental Research and Technology, Inc., Lexington, Massachusetts 02173
W. B. Lenoir
Johnson Spacecraft Center, National Aeronautics and Space Administration, Houston, Texas 77058

References and Notes

1. F. T. Barath, A. H. Barrett, J. Copeland, D. E. Jones, A. E. Lilley, *Astron. J.* **69**, 49 (1964).
2. A. E. Basharinov, A. S. Gurvich, S. T. Yegorov, *Dokl. Akad. Nauk SSSR* **188**, 1273 (1969).
3. P. W. Rosenkranz, F. T. Barath, J. C. Blinn III, E. J. Johnston, W. B. Lenoir, D. H. Staelin, J. W. Waters, *J. Geophys. Res.* **77**, 5833 (1972).
4. D. H. Staelin, *Proc. Inst. Electr. Electron. Eng.* **57**, 427 (1969).
5. ———, *J. Geophys. Res.* **71**, 2875 (1966).
6. T. Wilheit, W. Nordberg, J. Blinn, W. Campbell, A. Edgerton, *Remote Sensing Environ.* **2**, 129 (1973).
7. M. L. Meeks and A. E. Lilley, *J. Geophys. Res.* **68**, 1683 (1963).
8. We thank W. Nordberg for critical help in the establishment of this experimental program. We also thank J. C. Blinn III for help with the instrument calibration, and K. Kunzi, R. Pettyjohn, and R. K. L. Poon for developing many of the data-reduction computer programs. This work was suported by NASA contract NAS7-100.

14 August 1973

Micrometeorite Craters Discovered on Chondrule-Like Objects from Kapoeta Meteorite

Abstract. *Craters attributable to hypervelocity impacts of micrometeorites have been discovered on rare chondrule-like objects from the gas-rich meteorite Kapoeta. These chondrule-like objects, probably generated by impacts themselves, provide further evidence for the regolith origin of Kapoeta. The micrometeorite flux at the time of formation of the meteorites was probably an order of magnitude higher than the present flux, but the solar luminosity could not have been higher than 1.7 times its present value.*

The Kapoeta meteorite is a typical gas-rich meteorite which contains high concentrations of helium, neon, and argon. The rare gas excess is generally believed to be the result of solar wind implantation because it is confined to the outer ~ 10^{-5} cm of mineral grains (*1*) and has relative abundance ratios similar to those observed in the sun. Roughly 10 percent of the grains in Kapoeta are "track-rich" grains (*2, 3*) attributable to strong irradiation by low-energy (~ 1 Mev per nucleon) iron-group nuclei from solar flares. The density and radial gradient of tracks in the track-rich grains indicate that these grains were exposed to solar flare particles for times on the order of 10^4 years (*2, 3*), with negligible shielding ($<10^{-3}$ g cm^{-2}). The nonuniformity of the track density around the grain boundaries (*3, 4*) shows that the grains were partially shielded, probably by neighboring grains, during irradiation. The solar wind–implanted gas, the track-rich grains, the nonuniform grain irradiation, and the brecciated texture observed in Kapoeta are all seen in lunar soils and breccias (*5*).

Micrometeorite craters caused by the hypervelocity impact (> 4 km sec^{-1}) of interplanetary grains have been found on particles in all lunar soils examined. To investigate further the origin of gas-rich meteorites we examined surfaces of Kapoeta grains for micrometeorite craters. Two grams of Kapoeta were gently crushed to a 200-mesh size and optically examined for grains with surfaces smooth enough for crater searches with a scanning electron microscope (SEM); our search revealed a total of nine smooth spheroidal objects (> 100 μm). These are similar to the glass spheres found in lunar soils (*6*) and around some terrestrial impact craters (*7*).

Careful scanning of the spheres at high magnification in the SEM revealed that two of the spheres had microcraters. Sphere A-2 had 22 identifiable craters > 0.4 μm in diameter. Sphere B-1 had two craters > 0.4 μm. Figure 1 shows some of these microcraters. The well-defined spall zones and the smooth, glass-lined pit bottoms can be clearly seen. The microcraters found on the Kapoeta spheres are morphologically similar to craters on lunar glasses and to those produced in laboratory simulations. Craters larger than 4 μm in diameter have smooth glass-lined pits surrounded by spall zones of fractured glass, whereas craters with diameters less than ~ 4 μm consist of pits surrounded only by raised rims. The ratio of the spall zone diameter to the pit diameter for Kapoeta craters is the same as that observed for lunar microcraters. From the results of laboratory simulation experiments (*8*), we conclude that the observed crater morphology is due to the impact of projectiles with velocities in excess of 4 km sec^{-1}. The depth-diameter ratios and circularities of the Kapoeta craters are qualitatively similar to those of craters on lunar glasses. By comparison with microcraters produced by laboratory simulations (*9*), we deduce that, like lunar microcraters, the craters on Kapoeta were produced by rather equidimensional particles whose densities are consistent with those of ordinary silicate grains.

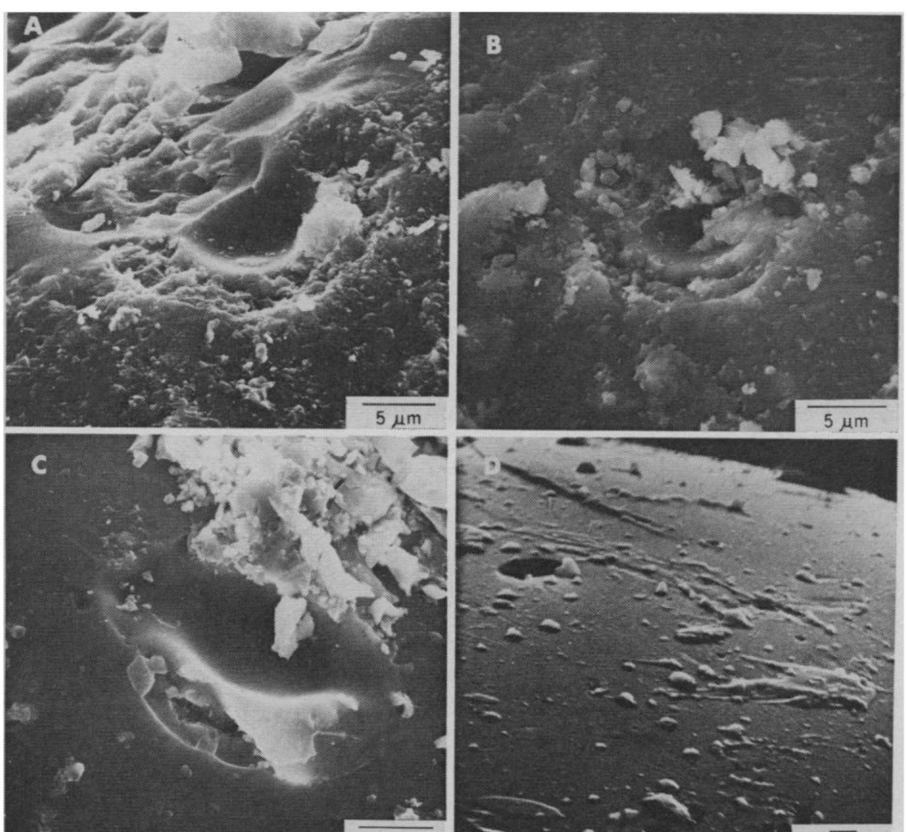

Fig. 1. Surface features of Kapoeta spheres. (A) Submicrometer-sized crater (lower left) and large crater with spall zone (center) on sphere A-2. The upper left portion of (A) is a fracture system not genetically related to the craters. (B) Spalled microcrater on sphere A-2 partially obscured by the Kapoeta matrix adhering to the sphere. (C) Spalled microcrater on sphere A-1. Note the ejecta splatter (top left) and lip structures (right). (D) Oblique view of sphere A-1 showing splatter features and gouges. Note the submicrometer-sized crater with a raised lip (top center).

The size distribution of craters on sphere A-2 is shown in Fig. 2 and is compared with that for the lunar glass surface 15286 (*9*). Craters as small as 0.15 μm in diameter were also seen on sphere A-2, and it is possible that the size distribution in Fig. 2 extends continuously down to 0.1 μm. Sphere B-1 had one 10-μm crater and one 1-μm crater. The deficiency of small craters on sphere B-1 can be interpreted as evidence of shielding by a thin layer (~ 10 μm) of dust. Small craters are deficient on some lunar surfaces and even on localized areas of surfaces with otherwise normal crater populations.

Micrometeoroids smaller than a certain critical size may have very short lifetimes (months) in the inner solar system owing to the influence of radiation pressure. The steepness and lack of a change of slope in the crater size distribution (Fig. 2) through the micrometer and submicrometer range show that there was no size cutoff in the micrometeorite flux attributable to radiation pressure at the time of formation of Kapoeta. Using Mie scattering theory, Gindilis *et al.* (*10*) have shown that, with the present luminosity of the sun, the centrifugal force due to solar radiation cannot exceed the centripetal force due to gravity for silicate grains of any size. The absence of a size cutoff due to radiation pressure enables us, utilizing the computations of Gindilis *et al.*, to set a limit on the luminosity of the sun at the time Kapoeta was formed. Assuming grains of pure silicate composition, we deduce that the solar luminosity could not have been more than 1.7 times its present value during the brecciation stage of Kapoeta's formation. On the basis of indirect evidence (*4*) and the observation that Kapoeta contains a rare gas component postulated to have been implanted by the pre-main sequence solar wind (*11*), we believe that Kapoeta was brecciated more than 4×10^9 years ago.

Studies of particle tracks in spheres A-2 and B-1 provide estimates of their exposure times to the ancient micrometeorite flux. Sphere B-1 has a low track density consistent with shielding, whereas sphere A-2 is a track-rich grain with a gradient. The measured density of tracks in sphere A-2 (5×10^8 cm^{-2}) at a depth of 10 μm is typical of about 100 irradiated grains studied in this meteorite (*2, 3*). Comparing our samples with lunar glass allows an estimation of the ancient micrometeorite flux. Because the absolute solar flare track density at a given depth is a measure of the exposure time, the ratio of crater density to track density is a measure of the micrometeoroid flux. By comparison with the lunar data of Neukum *et al.* (*12*), we find that

$$\left(\frac{N_c}{\rho}\right)_{\text{Kapoeta}} = 2.2 \times 10^{-5}$$

and

$$\left(\frac{N_c}{\rho}\right)_{\text{lunar glass}} = 2.6 \times 10^{-6}$$

where N_c is the cumulative density of craters larger than 1 μm and ρ is the density of tracks at a depth of 10 μm. Accordingly we infer that either the micrometeorite flux at the time of formation of the gas-rich meteorites was about an order of magnitude higher than that on the lunar surface at the present time, or the ancient solar flare flux was lower than it is at present. Although the flux of solar flare particles in the early solar system may not have been the same as today, it is believed that it might have been higher than the present value but that it could not have been lower (*13*). This would tend to increase the disparity in the micrometeoroid fluxes. Attenuation of the solar flare flux by interplanetary material is not a significant problem; otherwise, the observed track gradients would not extend to grain surfaces.

Apart from the existence of microcraters, the spheres in Kapoeta are of unusual interest in themselves and they have not previously been reported in the literature. They are not perfect spheres but have oblate and prolate shapes, a finding which suggests that they were once molten, rotating bodies. The surfaces of the spheres have dents, grooves, and splatter features (see Fig. 1D) similar to those commonly seen on lunar glass spheres (*6*). One of the spheres has a crystalline grain partially embedded in its surface which appears to have been implanted while the sphere was still plastic. The grain does not have the same composition as the sphere. Of the nine spheres, seven have crystalline interiors and are darkish brown to opaque. Of the two glass spheres, one is transparent with the shape of a broken dumbbell and the other (sphere B-1) is a nearly perfect sphere. It is not clear at present whether the Kapoeta spheres are related to chondrules. They do not closely resemble chondrules from ordinary chondritic meteorites; on the other hand, they do fit the description proposed by Fredriksson *et al.* (*14*) as a new definition of chondrules.

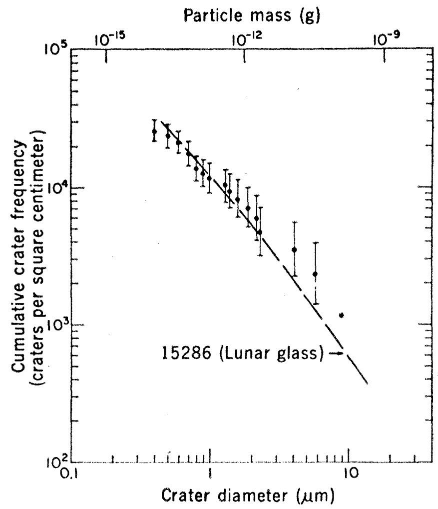

Fig. 2. Cumulative size frequency distribution of microcraters on Kapoeta sphere A-2 as compared with the lunar glass surface 15286 (*9*). Error bars indicate the counting statistics.

Qualitative x-ray analysis in the SEM showed that eight of the spheres had very similar compositions. A quantitative electron microprobe analysis carried out on one of these, sphere B-1, gave the following measured composition (in percentages by weight) for this green glass sphere: FeO, 18.6; MgO, 17.4; SiO_2, 46.9; Al_2O_3, 7.2; CaO, 8.7; TiO_2, 0.50; and Na_2O, 0.18. This composition is in good agreement with the bulk analysis for Kapoeta howardite by Müller and Zähringer (*15*). If we use the classification scheme of Mason (*16*), based on the CaO content and the ratio of FeO to (FeO + MgO) (in mole percentages), the sphere falls into the howardite group. The only serious discrepancy between our analytical data for the sphere and the bulk Kapoeta analysis lies in the sodium content, which is depleted by a factor of 3 in the sphere. Sodium depletion has been reported in some glass spheres found on the moon and around some terrestrial impact craters. Fredriksson *et al.* (*7*) have suggested that the sodium depletion is a result of selective vaporization and may be indicative of an impact origin. On the basis of chemical and morphological considerations, we believe that most of the spheres in Kapoeta are solidified droplets of shock-melted ejecta produced by cratering events on the Kapoeta parent body. The rarity of spheres in Kapoeta as compared with the lunar soil may be due to the smaller size of the Kapoeta parent body. On the other hand, the ability to retain any impact spheres at all implies the existence of surface gravity and places some lower limit on the size of the Kapoeta parent body. We feel that the presence of impact-generated spheres lends further support to the suggestion that Kapoeta formed on the surface of a body of asteroidal dimensions (*3, 17*). Evidence that Kapoeta was derived from an unusually large meteorite parent body comes from the discovery by Black (*11*) that Kapoeta contains a rare gas component not found in other analyzed meteorites but common in lunar soils and breccias. Black interprets this component as due to reimplanted atmospheric ions, a process which requires a sizable parent body.

In addition to textural and some chemical similarities, the presence in the Kapoeta achondrite of track-rich grains, an atmospheric rare gas component, glass spheres, and micrometeorite craters establishes that this achondrite is a remarkably close meteoritic analog to lunar soil breccias. Although other possibilities exist, we believe this is compelling evidence that, like most lunar rocks, Kapoeta was formed by impact processes on an impact-generated regolith. Various lines of evidence suggest that this regolith covered the surface of a sizable meteorite parent body. The isochemical nature of the spheres implies that the surface of the parent body was much more chemically homogeneous than the lunar surface and was therefore probably much smaller than the moon. The presence of solar flare tracks and craters caused by hypervelocity impacts of submicrometer-sized particles indicates that Kapoeta formed after the dissipation of the solar nebula, probably during the waning stages of the accretionary processes that formed the planetary bodies of the solar system. Most meteorites show signs of mechanical reworking, and they may also have resided in impact regoliths at some time during their histories. However, the absence of track-rich grains in many meteorites implies that either their residence time at the regolith surface was very short, or at the time of their formation the solar nebula shielded them from solar flare particles.

The existence of micrometeorite craters on meteoritic materials provides a means of studying properties of the dust component of the ancient solar system. On the basis of the work presented here, it appears that, although the flux may have been slightly higher in the past, the size distribution and physical properties of the interplanetary dust have not changed appreciably over most of the age of the solar system. Because it is generally believed that interplanetary grains are derived from comets, this implies a long-term stability to cometary phenomena in the inner solar system.

Note added in proof: From discussions with Noonan and Jeromé (*18*), we have learned that chondrule-like objects have recently been found in two other howardites: Bununu and Malvern.

D. E. BROWNLEE
Department of Astronomy, University of Washington, Seattle 98195

R. S. RAJAN
Department of Physics, University of California, Berkeley 94720

References and Notes

1. P. Eberhardt, J. Geiss, N. Grögler, *Tschermak's Mineral. Petrog. Mitt.* **10**, 535 (1965); H. Wanke, *Z. Naturforsch. A* **20**, 946 (1965).
2. D. Lal and R. S. Rajan, *Nature* **233**, 269 (1969); P. Pellas, G. Poupeau, J. C. Lorin, H. Reeves, J. Andouze, *ibid.*, p. 272.
3. R. S. Rajan, *Geochim. Cosmochim. Acta*, in press; D. Macdougall, R. S. Rajan, P. B. Price, *Science*, in press.
4. P. Pellas, in *From Plasma to Planet* (Nobel Symposium 21), A. Elvius, Ed. (Wiley, New York, 1972), p. 72.
5. D. Macdougall, R. S. Rajan, I. D. Hutcheon, P. B. Price, *Geochim. Cosmochim. Acta*, in press.
6. J. B. Hartung, F. Hörz, D. S. McKay, F. L. Baiamonte, *Moon* **5**, 436 (1972).
7. K. Fredriksson, A. Duke, D. J. Milton, M. S. Balasundaram, *Science* **180**, 862 (1973); P. W. Hodge and F. W. Wright, *J. Geophys. Res.* **76**, 3880 (1971).
8. J. F. Vedder, *Earth Planet. Sci. Lett.* **11**, 291 (1971).
9. D. E. Brownlee, F. Hörz, J. F. Vedder, D. E. Gault, J. B. Hartung, *Geochim. Cosmochim. Acta*, in press.
10. L. M. Gindilis, N. Divari, L. Reznova, *Sov. Astron. AJ* **13**, 114 (1969).
11. D. C. Black, *Geochim. Cosmochim. Acta* **36**, 347 (1972).
12. G. Neukum, E. Schneider, A. Mehl, D. Storzer, G. A. Wagner, H. Fechtig, M. R. Bloch, *Geochim. Cosmochim. Acta* **3** (Suppl. 3), 2793 (1972).
13. W. Fowler, J. Greenstein, F. Hoyle, *Geophys. J. Roy. Astron. Soc.* **6**, 148 (1962); R. Bernas, E. Gradsztajn, H. Reese, E. Schatzman, *Ann. Phys. N.Y.* **44**, 426 (1967).
14. K. Fredriksson, A. Noonan, J. Nelen, *Moon* **7**, 475 (1973).
15. O. Müller and J. Zähringer, *Earth Planet. Sci. Lett.* **1**, 25 (1966).
16. B. Mason, *Geochim. Cosmochim. Acta* **31**, 107 (1967).

E. Anders, *Space Sci. Rev.* **3**, 583 (1964); G. Poupeau and J. L. Berdot, *Earth Planet. Sci. Lett.* **14**, 281 (1972); L. Wilkening, thesis, University of California, San Diego (1970).

18. A. Noonan and D. Jeromé, personal communication.
19. We thank D. Lal for providing the Kapoeta sample. We thank P. B. Price and P. W. Hodge for their critical reading of the manuscript and D. E. Gault and F. Hörz for valuable suggestions. Research supported by NASA grants NGR 48-002-033 and NAL 05-003-410.

2 August 1973; revised 10 September 1973

Quantum Low-Temperature Limit of a Chemical Reaction Rate

Abstract. *The radiation-induced polymerization of formaldehyde has been studied in the solid state. The time of addition of one new link to a polymer chain increases exponentially in accordance with the Arrhenius law at 140 to 80 K, but approaches a constant value (approximately 10^{-2} second) at temperatures below 10 K. Thus, a low-temperature limit to a chemical reaction rate has been observed. It is interpreted as a quantum effect caused by tunneling from the zero vibration level of the initial state, and a semiquantitative theory is given. The phenomenon should be taken into account for understanding tunneling of electrons in biological systems when such tunneling is accompanied by conformational changes. It could also be significant in slow, exothermic chemical reactions at low and ultralow temperatures, which may have had a role in chemical and biological evolution (cold prehistory of life?).*

In a number of experiments (*1*) we have determined calorimetrically the time of growth of polymer chains for the radiation-induced solid state polymerization of formaldehyde at low temperatures (4 to 140 K). The polymerization at 77 to 140 K was induced by the bremsstrahlung of 5-Mev electrons from a linear accelerator; an adiabatic calorimeter with a relaxation time of 0.3 to 0.5 second was used. Below 77 K polymerization was induced by ^{60}Co gamma rays passing through a lead shield by means of a slit with a short opening time; the relaxation time of the diathermic calorimeter with Cu-Au-Fe thermocouples was 1 to 2 seconds.

Judging from the large radiation yields of polymerization ($G = \sim 10^7$ molecules per 100 ev at 140 K, $\sim 10^5$ at 77 K, and $\sim 10^3$ at 4 K), the role of radiation seems to be restricted to the formation of primary active centers—that is, to starting the polymer chain (which is endothermic). Once the chain starts, the formation of each new link is an exothermic process which can proceed spontaneously, without the participation of radiation.

The results are represented in Fig. 1, where $\tau_0 = \tau / G$ is the average time of addition of one new link to a polymer chain (τ is the measured time of growth of a whole chain, and the radiation yield of chain initiation is taken as ~ 1 for all temperatures). When the temperature decreases from 140 to 80 K, the value of τ_0 increases in accordance with the Arrhenius law with an activation energy $E \approx 0.1$ ev. At lower temperatures, however, we observe a strong deviation from the Arrhenius law and τ_0 approaching a constant value of approximately 10^{-2} second. An Arrhenius-type extrapolation would give a τ_0 of about 10^{30} years for 10 K and about 10^{100} years for 4 K.

Thus, a low-temperature limit to a chemical reaction rate has been observed for the radiation-induced polymerization of formaldehyde. Such a limit can only be of quantum origin, caused by tunneling from the zero vibrational level of the initial state. Also, such transitions are impossible for endothermic reactions.

Tunneling between two equal potential wells without a change of the system's energy has been treated for a Boltzmann continuous distribution and a quantum mechanical distribution (*2*). It was shown that for these simplified cases the reaction rate at low temperatures should reach some plateau value, determined by the parameters of the potential barrier (height, width, and shape) and by the tunneling mass. However, our present experimental case is more complicated because it involves transitions between two different wells, as illustrated in Fig. 2. Two effects must happen to establish a new link of the polymer chain: the molecule of formaldehyde must get closer, with the C–C distance changing from d_i to d_f ($d_i - d_f = \Delta d$), and the C=O bond must change from a double bond to a single bond. The growth of the polymer chain should involve either the transfer of an electron

$$\ldots CH_2–O–CH_2–O– + CH_2{=}O \rightarrow \ldots CH_2–O–CH_2–O–CH_2–O–$$

or the transfer of a hydrogen atom

$$\ldots CH_2–O–\overset{+}{C}H–\overset{-}{O}– + CH_2{=}O \rightarrow \ldots CH_2–O–CH_2–O–\overset{+}{C}H–\overset{-}{O}–$$

but in any case the transfer should be accompanied by (or should lead to) the approach of the formaldehyde molecule to the end group of the growing polymer. The tunneling of the whole formaldehyde molecule (mass M) is certainly much slower than electron tunneling, because of the large difference in their masses: $M/m \approx 5.5 \times 10^4$. It is not as easy to exclude